EARTH OBSERVATION AND GEOMATICS ENGINEERING
website: https://eoge.ut.ac.ir

Flood inundation modeling in ungauged basins using Unmanned Aerial Vehicles imagery

Adel Yavari[1,2,*], Saeid Homayouni[3], Khalid Oubennaceur[3], Karem Chokmani[3]

[1] Department of Civil Engineering, University of Qom, Qom, Iran
[2] Isfahan Province Water & Waste Water Company, Isfahan, Iran
[3] Institut National de la Recherche Scientifique, Centre Eau Terre Environnement, 490, rue de la Couronne Québec (QC) G1K 9A9, Canada

Article history:
Received: 10 January 2019, Received in revised form: 26 April 2020, Accepted: 2 May 2020

ABSTRACT

This paper presents a new framework for floodplain inundation modeling in an ungauged basin using unmanned aerial vehicles (UAVs) imagery. This method is based on the integrated analysis of high-resolution ortho-images and elevation data produced by the structure from motion (SfM) technology. To this end, the Flood-Level Marks (FLMs) were created from high-resolution UAV ortho-images and compared to the flood inundated areas simulated using the HEC-RAS hydraulic model. The flood quantiles for 25, 50, 100, and 200 return periods were then estimated by synthetic hydrographs using the Natural Resources Conservation Service (NRCS). The proposed method was applied to UAV image data collected from the Khosban village, in Taleghan County, Iran, in the ungauged sub-basin of the Khosban River. The study area is located along one kilometre of the river in the middle of the village. The results showed that the flood inundation areas modeled by the HEC-RAS were 33%, 19%, and 8% less than those estimated from the UAV's FLMs for 25, 50, and 100 years return periods, respectively. For return periods of 200 years, this difference was overestimated by more than 6%, compared to the UAV's FLM. The maximum flood depth in our four proposed scenarios of hydraulic models varied between 2.33 to 2.83 meters. These analyses showed that this method, based on the UAV imagery, is well suited to improve the hydraulic modeling for seasonal inundation in ungauged rivers, thus providing reliable support to flood mitigation strategies.

KEYWORDS

UAV Imagery and Mapping
Khosban-River
Flood-Level Marks
HEC-RAS
Flood Inundation
Ungagged Basin
Hydraulic Modelling

1. Introduction

Flood has been one of the natural hazards affecting human activities since the beginning of civilization and has always caused economic and human damage in many countries (Azizian, 2018; Yahya et al., 2010; Bernet et al., 2018; Domeneghetti et al., 2019). One of the strategies to reduce future flood risks is hydraulic modeling of streams in order to identify the flood risk areas (Li et al., 2018; Das, 2019; Golshan et al., 2016; Aishwaryalakshmi et al., 2017; Bezak et al., 2018; Merwade et al. 2008; Rahman &Ali, 2016, Zeleňáková et al., 2019). Heavy rainfalls or snow melting causes increase river water levels and flood risk (Sumalan et al., 2017). Torrential rains can occur even in arid and semi-arid regions with relatively low rainfall, causing seasonal floods. Therefore, monitoring surface-level flooding is essential for developing flood hazard zoning and mapping (Kirk, 2013). As a solution, hydraulic modeling is a useful and efficient tool in the simulation of floods. The spatial resolution and the geometric accuracy of topographic data may affect hydraulic flood modeling (Mourato et al., 2014).

Due to their impact on hydrograph and flood extent, modeling ground surfaces is critical for hydraulic simulation results. A hydraulic model with a high spatial resolution is particularly useful when large-scale processes have to be considered in predicting the model (Coveney & Roberts, 2017). For example, in complex environments, a high-resolution Digital Elevations Model (DEM) is essential for simulating floodplains (Mourato et al., 2014).

* Corresponding author
E-mail addresses: adel.yavari@aol.com (A. Yavari); saeid.homayouni@ete.inrs.ca (S. Homayouni); khalid.oubennaceur@ete.inrs.ca (Kh. Oubennaceur); karem.chokmani@ete.inrs.ca (K. Chokmani)

DOI: 10.22059/eoge.2020.297824.1075

A combination of ortho-mosaic images and DEM with high spatial resolution as inputs of hydrological models can result in a better 3D simulation of areas under the flood simulations with different intensities (Baggio & Rouquette, 2006). This 3D simulation provides an adequate understanding of the interactions between water and terrain surface and an accurate locating of flood-prone areas (Horritt et al., 2001; Mourato et al., 2014). The invention of remote sensing made a vital step for mapping impervious areas and landscape changes.

Most studies on the extraction of impervious surfaces from remote sensing data focused on satellite images (Weng, 2012). However, Some researchers have used high-resolution unmanned aerial vehicles (UAVs) imagery to monitor flood characteristics (Cook & Merwade, 2009; Geerling et al.,2009; Flener et al., 2013; Lee et al., 2013; Feng et al., 2015; Dietrich, 2016; Perks et al., 2016; Popescu et al., 2017; Hashemi-Beni et al., 2018; Rong et al., 2019; Şerban et al., 2016; Watanabe & Kawahara, 2016), hydrodynamic modeling (Yalcin, 2018), flood risk management (Hashemi-Beni et al., 2018), early warning systems (Schumann et al., 2019), and post-flood damage estimation (Zeleňáková et al., 2019). In hydrology, UAVs have a crucial role to characterize the surface flow quantitatively, allowing for remotely accessing the water body of interest. UAVs' spreading use paved the way for integrating drone technology and optical sensing, hydraulic data such as inundated areas, surface flow measurements, and water level estimations. This image-based technology is well suited in the framework of the Prediction in Ungauged Basins (PUB) decade as this method can be used to retrieve hydraulic data in ungauged sites (Sivapalan et al., 2003; Ridolfi et al., 2016; Niedzielski et al., 2016; Bandini et al., 2017; Tauro et al., 2014). Casado et al. (2015) used a framework based on UAV imagery to recognize hydro-morphological features from high-resolution aerial imagery using a new Artificial Neural Network (ANN) method. This method enhances UAV use for environmental politics and shows the high potential of ANN and high-resolution images to control and manage rivers (Casado et al., 2015). Diakakis et al. (2019) surveyed the flood area during and after the flood using a combination of systematic ground and aerial observation data with UAV aid to reconstruct the flood's essential physical and hydrological characteristics its impacts (Diakakis et al., 2019). Zazo et al. (2015) used Reduced Cost Aerial Precision Photogrammetry (RC-APP) technique, based on a motorized technology Ultra-light Aircraft Ultra-light Motor (ULM). This technique is applied in river engineering for the geometric modeling and risk assessment of floods (Zazo et al., 2015). Watanabe and Kawahara (2016) used UAV photogrammetry to monitor the changes in river topography and vegetation. The Digital Surface Model (DSM) calculated using this method efficiently represents the variations in topography and ground with a maximum error of 4 cm. In addition, the changes in DSM, before and after the flood, were due to vegetation cover on sand and gravel (Watanabe &Kawahara, 2016). Nguyen et al. (2020) proposed a novel modeling approach for spatial prediction of flash floods based on the tree intelligence-based CHAID (Chi-square Automatic Interaction Detector). In this method, a forest of tree intelligence constructed through the random subspace ensemble, and then, the swarm intelligence was employed to train and optimize the model (Neguyen et al., 2020). Research works present various techniques for detecting geomorphological effects (e.g., deforestation, population growth, land-use changes, etc.) on floodplain using UAV and satellite imagery (Langhammer & Vackova, 2018; Barasa & Perrera, 2018; Alexakis et al., 2014). Feng et al. (2015) presented a combinatorial method for flood inundation mapping using the Random Forest algorithm and analysis based on high-resolution drone images. The random forest consisted of 200 branches of the decision tree and was exploited to acquire flood inundation (Feng et al.,2015). The UAV offers a fast and accurate way to acquire aerial images at a relatively low cost with resolution and accuracy, typically in the range of a few cms. Compared to traditional remote sensing data, the UAV enables the rapid operation to obtain high-frequency multi-temporal and high-resolution images.

Tokarczyk et al. (2015) investigated the quality of digital elevation models (DEMs) generated using UAV imagery from urban drainage modeling applications and found that a realistic representation (resolution < 1 m) plays a fundamental role in surface flow modeling (Tokarczyk et al., 2015).

Ungagged basins have been challenging in developing countries for natural hazards and flood monitoring for many years. In particular, the lack of hydrometric and synoptic stations data is an essential limitation that affects the accuracy and reliability of hydrologic and hydraulic models. To this end, topographic information collected by the terrestrial surveying techniques, satellite imagery, or UAV photogrammetry is needed. This research proposed a framework to identify and map the areas under the flood risk using high-resolution ortho-images and DSM/DEM from UAV imagery in the ungagged basins.

This methodology helps experts consider large-scale processes in predicting hydraulic and hydrological modeling and provide details that are not recognizable by terrestrial surveying and mapping, and satellite imagery. For such an application, accurate topographic information that affects the river's flow regime and helps extract accurate FLMs is essential. This method can be very advantageous for small and seasonal rivers, where the catchment has no hydrological data. This approach is expected to provide substantial support to the monitoring and management of rivers and flood monitoring.

2. Case study and Methodology

2.1. Case study

This research area is one of the sub-basins of Taleghan County, located in the Alborz Province in Iran (Figure 1). The main imaged river is the Khosban River, with a length of 1 km. This region is located between longitudes 50 47’ 4.3” to 50 47’ 42.35” E and latitudes 36 11’ 44.6” to 36 12’ 15.82” N. The maximum and minimum elevations in the basin are 2095 and 1953 m, respectively, and the annual precipitation in the area is 540 to 610 mm.

2.2. Methodology

To predict the characteristic of a flood in a specified area, it is better to measure and record several floods that have occurred previously in the region, then by statistical analysis on the hydrometric data, the most probabilistic floods that will occur in the future will be predicted. In cases where this data is not available, the use of empirical relationships, regional analysis, logical methods, or push the curve number method is an alternative (Alizadeh, 2011). Since no hydrometric stations were available in the study area, we used the Natural Resources Conservation Service and synthetic unit hydrograph of NRCS methods to estimate the flood discharges with 25, 50, 100, and 200 years of return. The NRCS method uses a hypothetical design storm and an empirical nonlinear runoff equation to compute runoff volumes and a dimensionless unit hydrograph to convert the volumes into runoff hydrographs. The methodology is particularly useful for comparing pre- and post-development peak rates, volumes, and hydrographs. The NRCS runoff equation’s critical component is the NRCS Curve Number (CN), based on soil permeability, surface cover, hydrologic condition, and antecedent moisture. Watershed or drainage area time of concentration is the crucial component of the dimensionless unit hydrograph. Figure 2 shows an overview of the processing and simulation workflow of flood inundation modeling in the Khosban River.

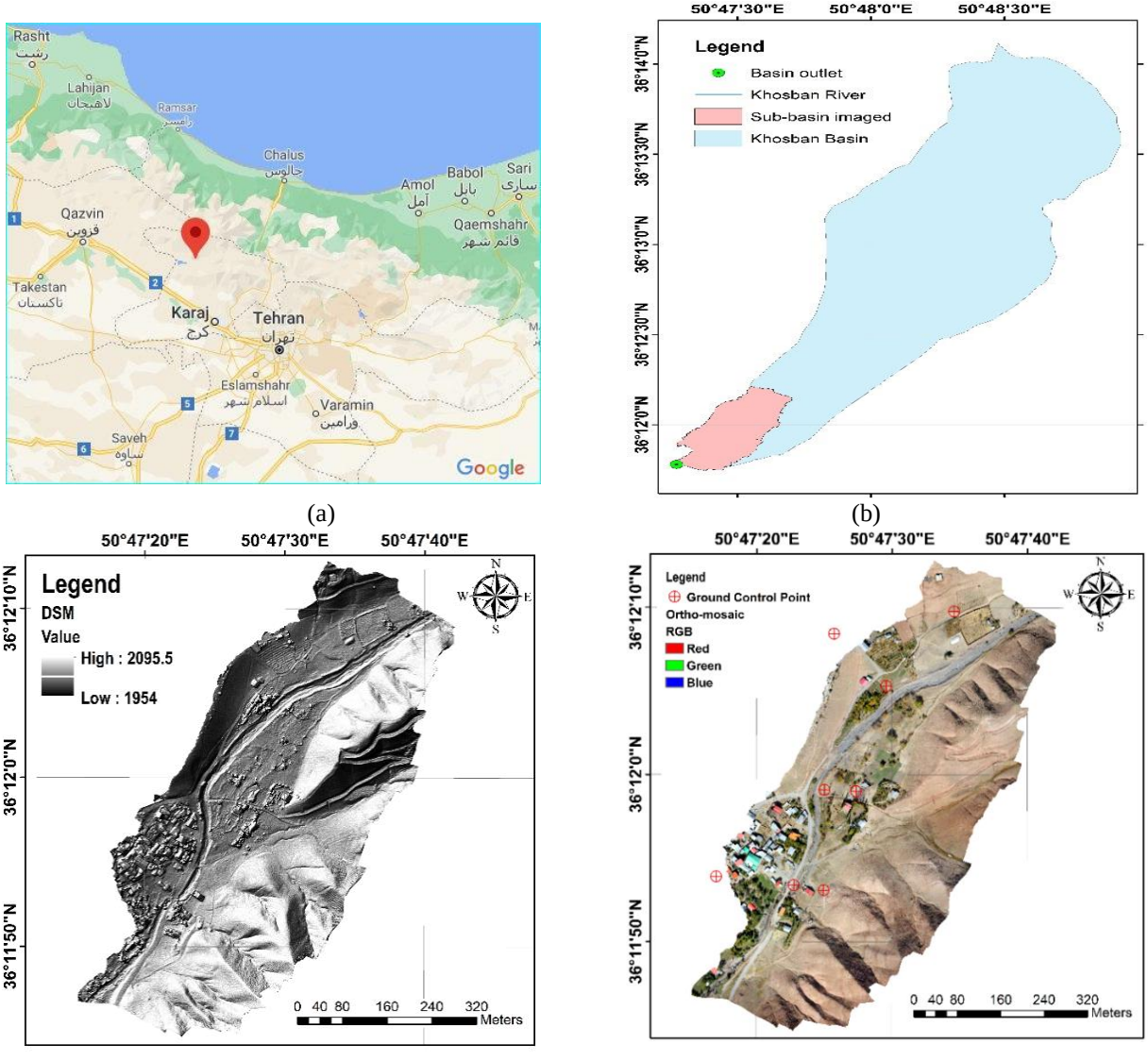

Figure 1. location of the Khosban River watershed in Iran (a); location of the Khosban basin and simulated flood area by UAV (b); the digital surface model (c); and the ortho-mosaic of the study area (d)

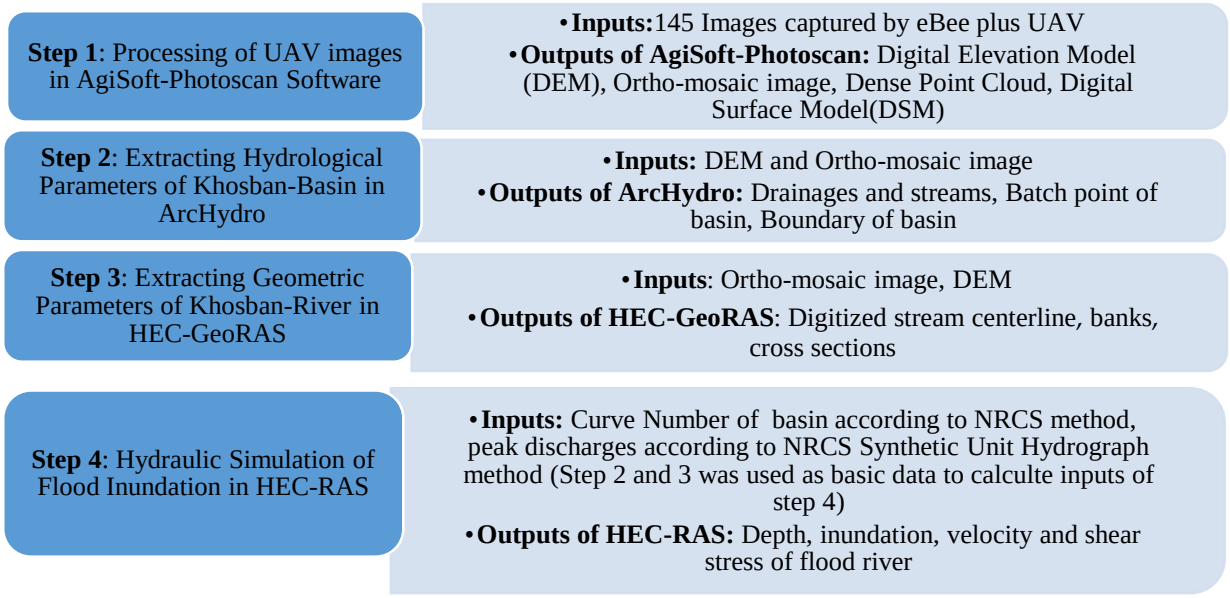

Figure 2. A general overview of the workflow in flood inundation of the Khosban River

The workflow starts with the processing of UAV images in AgiSoft Photoscan Software, recently renamed to Metashape (www.agisoft.com). Agisoft PhotoScan is a 3D modeling software that is capable of creating outputs that can be compared to those of the other software. To extract the hydrologic parameters of the catchment, the outputs of the AgiSoft-PhotoScan, including ortho-mosaic image and DEM, were used in ArcHydro. In addition, the HEC-GeoRAS extension of ArcGIS 10.5 developed by the Hydrologic Engineering Center (HEC) of the United States Army Corps of Engineers Hydrologic Engineering Center was used to produce the geometric parameters of the river that was imported into HEC-RAS. The flood discharge was estimated using the Win-TR55 software and based on different return periods of 6-hour rainfall in Storm-water Management and Design Aid (SMADA) software. Moreover, the Curve Numbers (CNs) of the basin were extracted using the Normalized Difference Vegetation Index (NDVI) from satellite images. Finally, the flood inundation modeled by 25, 50, 100, and 200 years return periods in HEC-RAS, and in the following, they were entered in the GIS environment to differentiate with Flood-Level Mark of the river that delineated from UAV images and TIN as observation data.

2.2.1. UAV Image Processing

To estimate and evaluate the mapping's accuracy using UAV images, Nama Pardaz Rayaneh (NPR) Company carried out an experimental project in Khosban Village in the spring of 2017 (www.nprco.com). The study area was imaged using a fixed-wing eBee Plus UAV system from SenseFly (https://www.sensefly.com). In a 24-minute flight and with a longitudinal and lateral overlap of 75 and 65 percent, respectively, a total of 145 photographs with a Ground Sample Distance (GSD) of 5 cm were collected at a flight height of 239 meters. The images cover an area of about 44.9 hectares covered by the UAV. This system is equipped with a Real-Time Kinematic and Post Processed Kinematic (RTK/PPK) positioning system. Therefore, the images captured by the photographic camera of this system, i.e., Sensor Optimized for Drone Applications (SODA), have a positional accuracy of about 2 cm. In addition, eight Ground Control Points (GCP) were measured in the area using a dual-frequency GPS receiver to ensure coincidence of positioning. These points were used as reference points to retrieve the geometric accuracy of the final geospatial output products. Table 1 shows the results of horizontal and vertical accuracies calculated on GCPs.

The collection images were processed using the Agisoft PhotoScan software based on the structure from motion (SFM) technology. The outputs from this step are a dense-point cloud model with more than 17 million points. From this point cloud, a digital elevation model with a pixel size of 5 cm was extracted. It should be noted that using dense DSM points, the clouds of trees were removed to create the Digital Train Model (DTM). The DTM and the ortho-mosaic map were used to model the physical and hydrological parameters of the river.

2.2.2. Hydrologic Parameters Extraction

To extract hydrological parameters of the region, ArcHydro and HEC-GeoHMS (Geospatial Hydrologic Modeling System) tools were used. These tools allow visualizing spatial information and extracting the properties of the basin from a DEM. There are various geomorphological forms, such as ditches, which may be identified as basin outlets. Therefore, before the process starts, these objects should be filled by preprocessing the DEM. To this end, the delineated FLMs from the UAV ortho-image should be used along with DEM to identify the

drainage streams in a basin. This operation is called DEM Reconditioning in ArcHydro, where the minor-streams are excluded through this function. After this operation, the thalwegs will then be represented visibly. This procedure implements the AGREE method developed by the Center for Research in Water Resources, the University of Texas at Austin (The university of texas at Austin, 1997). In the next step, regions in which the waterway feeds on the basin-scale must be outlined. These drainage areas were calculated automatically by ArcGIS. Finally, the basin outlet should be introduced to the software to close the basin boundary (The university of texas at Austin, 1997). Figure 3 shows the boundary and drainages of the sub-basin.

Table 1. The UTM coordinate (m) and accuracy of the ground reference points.

Longitude	Latitude	Altitude	Check Point	Error X	Error	Error Z
4006412.335	481164.962	2003.309	1	-0.014	-0.017	0.035
4006315.453	481261.089	2002.167	2	-0.003	-.007	0.011
4006124.161	481147.317	1987.906	3	-0.011	-0.011	-0.060
4006121.923	481205.036	1989.978	4	-0.014	-0.005	-0.010
4005948.815	481090.31	1976.321	5	-0.034	0.00	0.005
4006453.082	481386.528	2014.735	6	-0.020	-0.005	-0.014
4005964.885	480947.369	1982.66	7	-0.001	-0.025	-0.026
4005939.367	481145.824	1981.183	8	-0.040	-0.005	0.025
			Mean	-0.017	-0.009	-0.0043
			Sigma (m)	0.0129	0.077	0.028
			RMS Error (m)	0.0215	0.012	0.0287

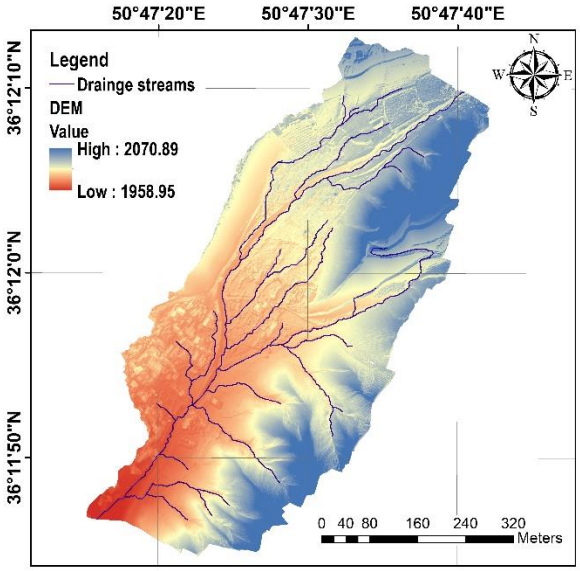

Figure 3. The boundary and drainage of the Khosban River sub-basin extracted using ArcHydro

2.2.3. River Hydraulic Simulation

The use of GIS for hydraulic and hydrological modeling usually requires three steps: 1- preprocessing of data 2- Running the model and output from HecGeo-RAS and HecGeo-HMS 3- Processing of information in HEC-RAS.

The HEC-GeoRAS extension was used to analyze the river data and to simulate the flood area. This extension can calculate surface profiles and water velocity and can be applied to flood zoning, flood damage calculations, and response. The primary data required for the HEC-GeoRAS extension is DEM or Triangular Irregular Network (TIN). To calculate the Manning's roughness coefficients, the land-use/land-cover classes extracted from the ortho-image map were used as the model (Cameron & Ackerman, 2013).

The geometric data generated in HEC-GeoRAS include the river centerline, cross-section, obstacles in the stream, weak flow areas, and land-use (Cameron & Ackerman, 2013). Since this river is seasonal, the river's bed was visible in the UAV imagery. Therefore, the thalweg of the river was manually drawn from the ortho-image and inputted into the model. Thanks to the visibility of this seasonal river's watermarks in the UAV images, the floodgate area was used to create the coastline layer. Therefore, the watermarks of flood lines were considered as the bank lines. Since the studied basin does not have the hydrometric station, the American Natural Resources Conservation Service (NRCS) method was used to estimate the flood discharge. It uses a hypothetical design storm and an empirical nonlinear runoff equation to compute runoff volumes and a dimensionless unit hydrograph to convert the

volumes into runoff hydrographs. The methodology is particularly useful for comparing pre- and post-development peak rates, volumes, and hydrographs. The NRCS runoff equation's critical component is the NRCS curve number (CN), based on soil permeability, surface cover, hydrologic condition, and antecedent moisture. Watershed or drainage area time of concentration is the critical component of the dimensionless unit hydrograph. One of the advantages of using this research is using high-resolution and high-accuracy UAV imagery-based DEM, DSM, and ortho-mosaic products with a 5-centimetre GSD and better than 5 cm of geo-referencing accuracy. In addition to the bare ground's elevation values, a DSM contains other objects such as buildings, trees, and other vegetation. As a result, DSM can be used as the basis for reliable and accurate collecting of the river cross-sections and the flood-level marks to compare with hydraulic modeling. Such relevant information for small riverbeds simulation is rare or very difficult to provide by the operational satellite sensors due to low spatial resolution (e.g., 5 to 15 meters).

The NRCS method is the most comprehensive model, which uses rainfall statistics rather than flood hydrographs. Since, in most cases, the meteorological stations' network is denser than the hydrometric stations, at least if there is no flood data, the rainfall statistics will be available. In this method, rainfall statistics used to get flood hydrographs (Nasiri & Alipur, 2014). On the other hand, in the NRCS synthetic unit hydrograph method, a maximum 24-hr rainfall was used since most meteorological stations record 24-hr rainfall data (Alizadeh, 2011). The basin's concentration-time was 22.6 minutes using the Kirpich Eq. (7) (Kamath et al., 2012; Salimi et al., 2017). Based on the NRCS method, if the concentration-time is under 6 hours, the design rainfall must be considered 6-hr rainfall. This rainfall time was calculated using Eq. (1) (Alizadeh, 2011).

$$P_{6,T} = \frac{P_{24,T}}{1.48} \quad (1)$$

where $P_{24,T}$ and $P_{6,T}$ are the 24-hr and 6-hr rainfall with T year return period, respectively.

The NRCS method models the discharge of flood widely used in hydrology, drainage, and surface water collection. This method assumes that Eq. (2) exists between runoff and water accumulation on the ground.

$$\frac{P - I_a - Q_d}{S} = \frac{Q_d}{P - I_a} \quad (2)$$

Where P is the amount of precipitation, I_a is the initial rainfall losses, including interception drain, depression storage, and infiltration, S is the maximum or potential of keeping moisture on the ground, and Q_d is the runoff height in the basin, all in centimetre. In Eq. (3), usually, precipitation losses are estimated 10 to 30 percent of the potential retention or about 0.1S to 0.3S, usually assumed to be equal 0.2S. Eq. (3) was obtained from Eq. (2), usually used by experts (Alizadeh, 2011).

$$Q_d = \frac{(P - 0.2S)^2}{(P + 0.8S)} \quad (3)$$

The value of S also depends on CN, and its value is according to Eq. (4) in the metric system.

$$CN = \frac{2540}{25.4 + S} \quad (4)$$

The geology map at the 1:250,000 scale and Landsat-8 were used to calculate CN. The $NDVI$ values were classified according to Table 3 into four categories; the values greater than 0.65 represent forests, the values ranging from 0.57 to 0.65 rangelands, 0.40 to 0.57 farmlands, and those less than 0.40 show the surfaces without cover vegetation. Each class was again subdivided into several sub-classes based on the Fractional Vegetation Cover (FVC) index, according to Eq. (6). When the FVC index is more significant than 0.75 is considered a healthy condition if the index is between 0.5 and 0.75 as a suitable condition and if the index is less than 0.5 considered an unsatisfactory condition (Salimi Kouchi et al., 2013). In the Taleghan dam basin, the soil type was classified according to Table 2.

$$NDVI = \frac{NIR - RED}{NIR + RED} \quad (5)$$

$$FVC = \frac{NDVI - NDVI_0}{NDVI_\infty - NDVI_0} \quad (6)$$

Table 2. Hydrologic Group Soils of the Taleghan dam basin

Type of Soil	Hydrologic Group of Soil
Inceptisols	A
Mollisols	C
Rock Outcrops/Ent isols	D

In Eq. (5), NIR and RED are the near-infrared and red band, respectively, equal to bands 5 and 4 of the Landsat-8 satellite. $NDVI_0$ is also $NDVI$ for bare soil, and $NDVI_\infty$ is the $NDVI$ index for vegetation that is considered the maximum NDVI value (Salimi Kouchi et al., 2013). The basin curve number was obtained based on $NDVI$ and FVC and a hydrologic group of the soil, according to Table 3.

One of the model's critical parameters is the Concentration Time (T_c) of the basin and is defined as the maximum time that the water from the farthest point of the basin has travelled its hydrological route to reach the outlet point. The concentration-time was calculated using the Kripich equation according to Eq. (7).

$$T_C \quad 0.0078 \frac{L^{0.77}}{S^{0.385}} \quad (7)$$

In the above equation, *L* is the most significant length of the basin's waterway in meters, and S is the mean slope of the basin. The concentration-time of the basin was acquired using Eq. (7), as 22.6 minutes. The flood discharges of the selected return period: 25, 50, 100, and 200 years were estimated using the flood frequency analysis which acquired 24.44, 35.89, 49.82, and 66.49 cubic meters per second, respectively. Synthetic hydrographs of the flood were acquired based on 6-hr rainfall, according to Figure 4. Flood inundation simulation was performed using a steady flow with a peak flow discharge of flood hydrograph and is shown in Figure 5.

,

Table 3. Basin Curve Number based on NDVI and FVC indexes (Fan et al., 2013)

Vegetation	**NDVI**	**Vegetation Vigor**	**Hydrologic Group**			
			A	B	C	D
Forest	NDVI>0.65	Poor: V<50%	45	66	77	83
		Fair: 50%<V<75%	36	60	73	79
		Good: V>75%	30	55	70	77
Grass and Bush	0.57<NDVI<0.65	Poor: V<50%	57	73	82	86
		Fair: 50%<V<75%	43	65	76	82
		Good: V>75%	32	58	72	79
Farmland	0.4<NDVI<0.57	Poor: V<50%	72	81	88	91
		Good: V>50%	67	78	85	89
None-Vegetated	NDVI<0.4		59	74	82	86

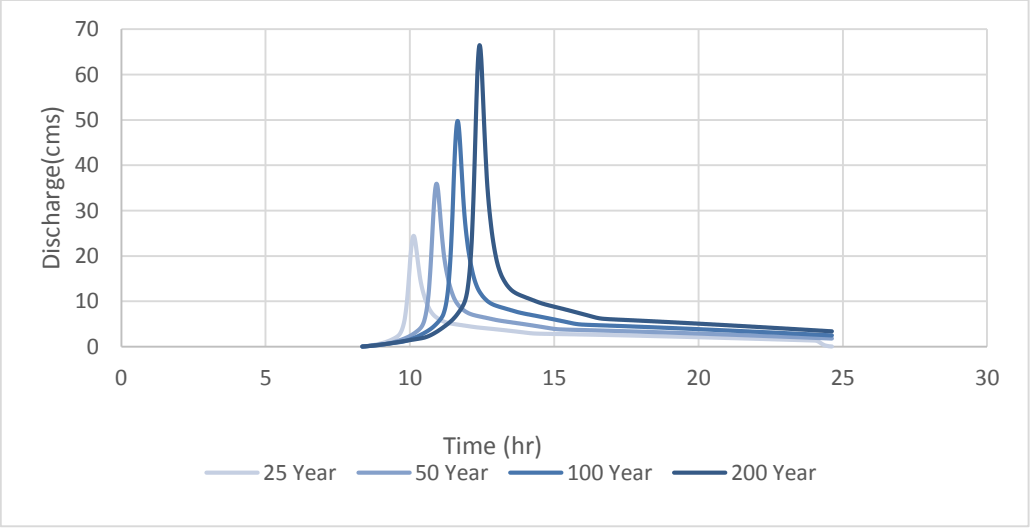

Figure 4. Synthetic hydrograph of floods with 25, 50, 100, and 200 years return period

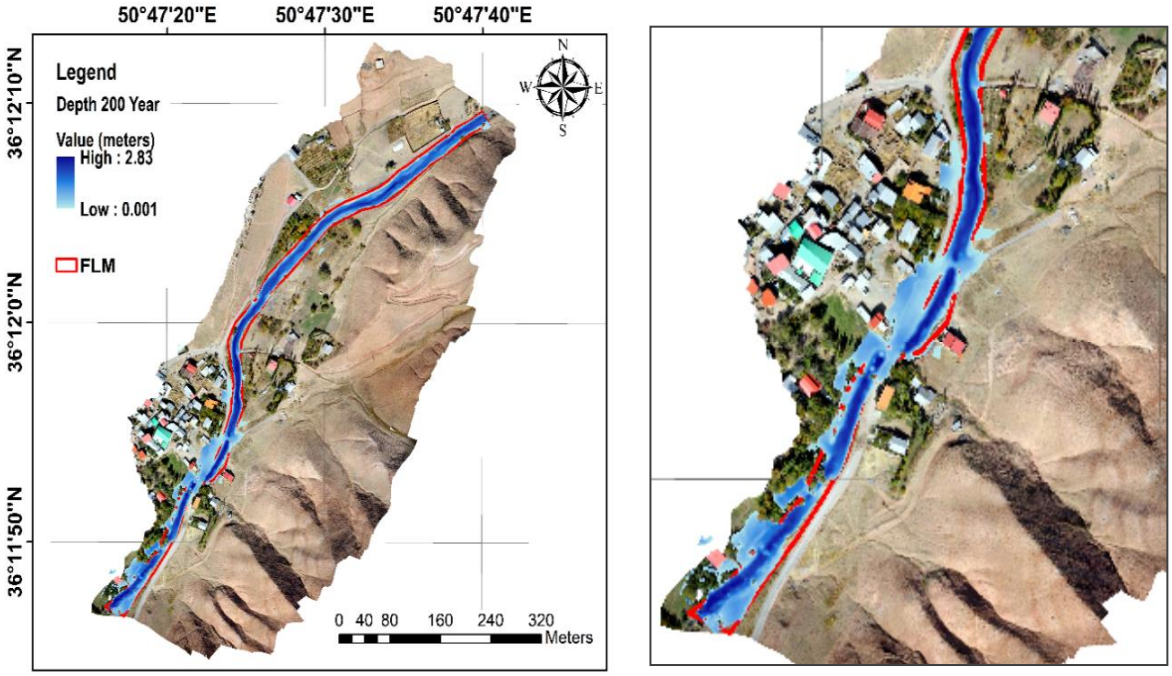

(a) (b)

Figure 5. The flood inundation of 200 years of the Khosban River and the companion with the FLM (a), and a zoom on the residential area (b)

3. Results and Discussion

Due to the limitations in common data sources, a combination of the spatial data products based on photogrammetric images of UAV, DEM, and the extracted spatial features are used to detect different flood conditions. Hydraulic modeling of the river surface profile is based on a steady flow; this system can be used for all channels or single branch rivers. This simulation can be done for the subcritical, supercritical, and mixed flow regimes. The computation method is based on solving the one dimensional energy equation. The energy loss was evaluated due to friction (the Manning equation) and expansion/contraction multiplied by the velocity head change. The momentum equation is used for conditions where the water velocity profile is changing rapidly. These conditions include mixed flow regime calculations (hydraulic jump), hydraulics of bridges, and calculating the profile at the rivers' intersection. The effect of various obstacles such as bridges/culvert, dams, overflow, and other structures may be considered in calculating the flood zonation. A steady flow system is designed for or application in flood plain management. Also, there is the capability to evaluate water surface profile changes due to repair canals and embankments (Brunner 2010).

The hydraulic modeling was performed for four discharges that were acquired based on estimates of peak flow. The free surface width of the stream in contact with free air along the river is shown according to Figure 6.

The hydraulic depth is the ratio of the cross section area of the stream (A) to the free surface width (T), calculated by Eq. (8). Figure 7 shows the hydraulic depth of water in the Khosban River.

$$\text{Hydraulic Depth} \quad \frac{A}{T} \tag{8}$$

In this study, the created watermark flood was taken from UAV and TIN's ortho-mosaic image as observation data compared with hydraulic modeled according to different return period discharges. The processes illustrated that the flood area extracted by the watermark in RGB images, modeling based on 25, 50, 100, and 200 years return period were 1.778, 1.195, 1.443, 1.643, and 1.890 acres, respectively. These areas, modeled by the HEC RAS, represent 33%, 19%, and 8% less difference compared to the FLM for 25, 50, and 100 years return periods, respectively. While for 200 years of the return period, this difference was overestimated by more than 6% compared to the FLM. Moreover, the maximum depth of flood in the hydraulic modeling performed with four scenarios varies between 2.33 and 2.83 meters.

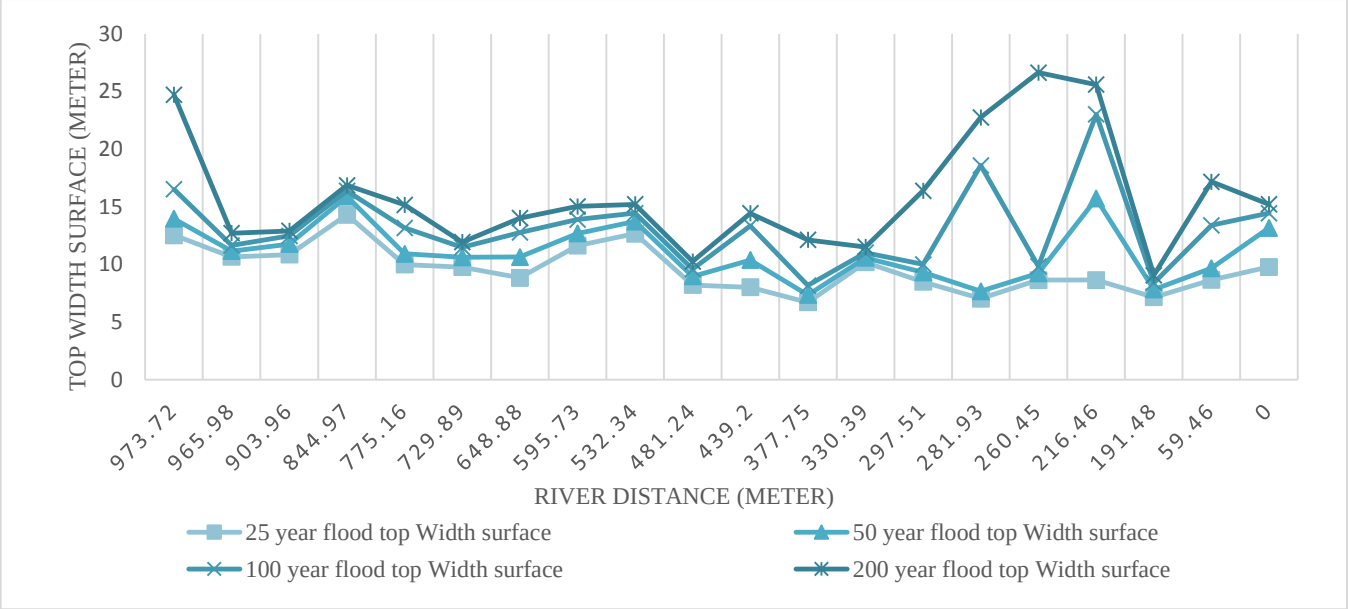

Figure 6. The free surface width of floods along the Khosban River

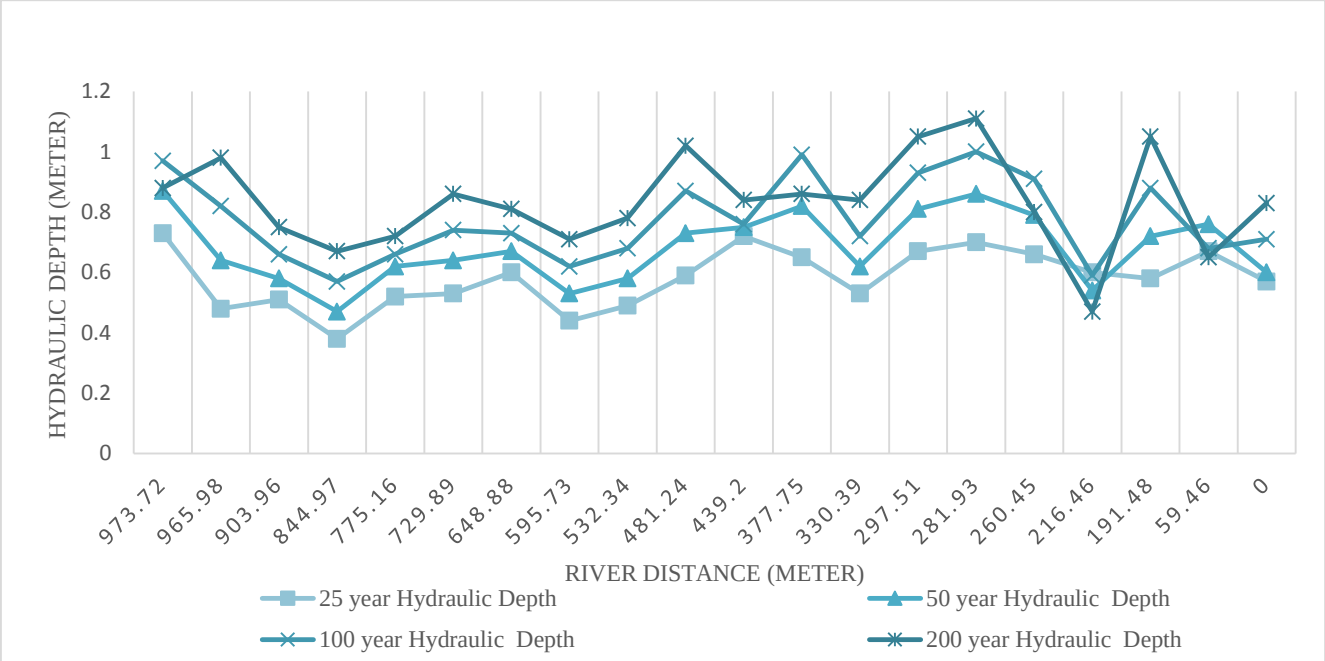

Figure 7. Hydraulic depth of water (in meters) along the Khosban River

4. Conclusion

Small rivers with a width smaller than 100 meters require land surveying or aerial images to delineate the small rivers' geometric parameters. The use of satellite imagery due to the low spatial resolution cannot lead to solid modeling. Consequently, the UAV imagery is essential to observe and map the river's topographic and hydrological details.

This paper proposed a novel methodology for floodplain inundation modeling based on a UAV system's high-resolution imagery. Several products, including points cloud, DSM, DEM, and orthophoto maps, were extracted using the Structure from the Motion technology and were used for this modeling. In this study, high-resolution UAV data collected from the Khosban Village near the Taleghan Dam. The Khosban River is seasonal and was dry during the image acquisition mission.

The flood zonation of the Khosban River is of high importance due to the average annual precipitation of over 500 mm and the presence of springs and mountainous peaks, and the flow of the river from the middle of the village residential houses. Since basins do not have enough statistical data, and there is no hydrometric station in the study area, the use of logical methods, curve push, regional analysis, or empirical relationships is inevitable. In this research, the basin curve number obtained using the Landsat-8 satellite and the UAV imagery, and geologic maps using the NRCS method provided by NRCS.

In this project, the river's cross-section was taken with 5 cm GSD, and hydrological characteristics and geometric parameters were modeled. The flood simulation showed that a part of the residential texture would be submerged caused by flood, and there is a need to review and implement river engineering measures to prevent a flood from entering residential buildings. Also, since rivers' banks are considered national territories and personal abuse cause contravention of the river margins, flood inundation can determine the river bank and prevent the riverside's illegal possession. The estimated flood area based on 6-hr rainfall and synthetic hydrograph of floods with 25, 50, 100, and 200 years of return period were 1.195, 1.443, 1.643, and 1.890 square meters. As can be seen, the hydraulic simulation of 200 years returns period of flood has the most adjustments with flood areas of FLM.

Acknowledgments

The authors thank Mr. Mehdi Boroumand, Nama Pardaz Rayaneh Company, and field crews for providing eBee Plus SenseFly images of the Khosban River used in this research.

References

Aishwaryalakshmi, V., Kumar, N., Prathap, M.G., & Abinaya, B. (2017). Flood inundation mapping for Sathanur Dam. *International Journal of Civil Engineering and Technology*. 8, 1306-1311.

Alexakis, D.D, Grillakis, M.G., Koutroulis, A.G., Agapiou, A., Themistocleous, K., Tsanis, I.K., & alis, A. (2014). GIS and remote sensing techniques for the assessment of land use change impact on flood hydrology: the case study of Yialias basin in Cyprus. *Natural Hazards and Earth System Sciences*. 14, 413-426.

Alizadeh, A. (2011). Principles of applied hydrology, *Astan Quds Razavi*: Mashhad, Iran.

Azizian, A. (2018). Investigating the application of remote sensing-based dams on for inundation mapping and hydraulic modeling. *Iran-Water Resources Research*.14, 212-223.

Baggio, S., & Rouquette, M.L. (2006). The Social Representation of the Flood: The Overlapping Influence of Proximity to Risk and the Importance of the Stake. *Bulletin de psychologie*, 1, 103-117.

Bandini, F., Jakobsen, J., Olesen, D., Reyna-Gutierrez, J.A.,& Bauer-Gottwein, P. (2017). Measuring water level in rivers and lakes from lightweight Unmanned Aerial Vehicles. *Journal of Hydrology*. 548, 237-250.

Barasa, B.N., & Perera, E.D.P. (2018). Analysis of land use change impacts on flash flood occurrences in the Sosiani River basin Kenya. *International journal of river basin management.* 16, 179-188.

Bernet, D.B., Zischg, A.P., Prasuhn, V., & Weingartner, R. (2018). Modeling the extent of surface water floods in rural areas: Lessons learned from the application of various uncalibrated models. *Environmental modelling & software.* 109, 134-151.

Bezak, N., Šraj, M., Rusjan, S., & Mikoš, M. (2018). Impact of the Rainfall Duration and Temporal Rainfall Distribution Defined Using the Huff Curves on the Hydraulic Flood Modelling Results. *Geosciences*. 8, 69.

Brunner, G.W. (2010). HEC-RAS River Analysis System User's Manual Version 4.1. *US Army Corps of Engineers Institute for Water Resources Hydrologic Engineering Center (HEC)*, California, USA.

Cameron, T., & Ackerman, PE. (2013). HEC-GeoRAS GIS Tools for Support of HEC-RAS using ArcGIS. Hydrologic Engineering Center: *extraído de*, USA.

Casado, M.R., Gonzalez, R.B., Kriechbaumer, T., & Veal, A. (2015). Automated identification of river hydromorphological features using UAV high resolution aerial imagery. *Sensors*. 15, 27969-27989.

Cook, A., & Merwade, V. (2009). Effect of topographic data, geometric configuration and modeling approach on flood inundation mapping. *Journal of Hydrology*, 377, 131-142.

Coveney, S., & Roberts, K. (2017). Lightweight UAV digital elevation models and orthoimagery for environmental applications: data accuracy evaluation and potential for river flood risk modelling. *International journal of remote sensing.* 38, 3159-3180.

Das, S. (2019). Geospatial mapping of flood susceptibility and hydro-geomorphic response to the floods in Ulhas basin, India. Remote Sensing Applications: *Society and Environment*.14, 60-74.

Diakakis, M., Andreadakis, E., Nikolopoulos, E.I., Spyrou, N.I., Gogou, M.E., Deligiannakis, G., & Tsaprouni, K. (2019). An integrated approach of ground and aerial observations in flash flood disaster investigations. The case of the 2017 Mandra flash flood in Greece. *International Journal of Disaster Risk Reduction*. 33, 290-309.

Dietrich, J.T. (2016). Riverscape mapping with helicopter-based Structure-from-Motion photogrammetry. *Geomorphology*. 252, 144-157.

Domeneghetti, A., Schumann, G.J.P., & Tarpanelli, A. (2019). Preface: Remote Sensing for Flood Mapping and Monitoring of Flood Dynamics. *Remote Sensing*, 11, 943.

Fan, F., Deng, Y., Hu, X., & Weng, Q. (2013). Estimating composite curve number using an improved SCS-CN method with remotely sensed variables in Guangzhou, China. *Remote Sensing*. 5, 1425-143.

Feng, Q., Liu, J., & Gong, J. (2015). Urban flood mapping based on unmanned aerial vehicle remote sensing and random forest classifier—A case of Yuyao, China. *Water*. 7, 1437-1455.

Flener, C., Vaaja, M., Jaakkola, A., Krooks, A., Kaartinen, H., Kukko, A., & Alho, P. (2013). Seamless mapping of river channels at high resolution using mobile LiDAR and UAV-photography. *Remote Sensing*. 5, 6382-6407.

Geerling, G.W., Vreeken- Buijs, M.J., Jesse, P., Ragas, A.M.J., & Smits, A.J.M. (2009). Mapping river floodplain ecotopes by segmentation of spectral (CASI) and structural (LiDAR) remote sensing data. *River research and applications*. 25, 795-813.

Golshan, M., Jahanshahi, A., & Afzali, A. (2016). Flood hazard zoning using HEC-RAS in GIS environment and impact of Manning roughness coefficient changes on flood zones in Semi-arid climate. *Desert*. 21, 24-34.

Hashemi-Beni, L., Jones, J., Thompson, G., Johnson, C., & Gebrehiwot, A. (2018). Challenges and opportunities for UAV-based digital elevation model generation for flood-risk management: A case of princeville, north carolina. *Sensors*. 18, 3843.

Horritt, M.S., & Bates, P.D. (2001). Effects of spatial resolution on a raster-based model of flood flow. *Journal of Hydrology*. 253, 239-249.

Kamath, A.M., Varun, V.M., Dwarakish, G.S., Kavyashree, B., & Shwetha, H.R. (2012). Soil loss estimation through MUSLE using Kirpich and Williams times of concentration using RS and GIS techniques: a case study. *ISH Journal of Hydraulic Engineering*, 18, 1-10.

Kirk, J. A. (2013). Methodology for Developing GIS-based Probabilistic Riverine Flood Inundation Maps for Tonawanda Creek in Western New York. *Doctoral dissertation degree*, Kent State University.

Langhammer, J., & Vackova, T. (2018). Detection and Mapping of the Geomorphic Effects of Flooding Using UAV Photogrammetry. *Pure and Applied Geophysics*. 175, 3223-3245.

Lee, I., Kang, J., & Seo, G. (2013). Applicability analysis of ultra-light UAV for flooding site survey in South Korea. *Remote Sensing and Spatial Information Sciences*. 40, 185-189.

Li, J., Li, J., & Yao, K. (2018). Inundation Analysis of Reservoir Flood Based on Computer-Aided Design (CAD) and Digital Elevation Model (DEM). *Water*.10, 530.

Merwade, V., Olivera, F., Arabi, M., & Edleman, S. (2008). Uncertainty in flood inundation mapping: current issues and future directions. *Journal of Hydrologic Engineering*. 13(7): 608-620.

Merwade, V. (2012). Stream network and watershed delineation using spatial analyst hydrology tools. *School of Civil Engineering, Purdue University*.

Mourato, S., Fernandez, P., Pereira, L., & Moreira, M. (2017). Improving a DSM Obtained by Unmanned Aerial Vehicles for Flood Modelling. *In IOP Conference Series: Earth and Environmental Science*.

Nasiri, A., & Alipur, H. (2014). Determination the Curve Number Catchment by Using GIS and Remote Sensing. Int. *Journal of Environmental, Chemical, Ecological, Geological and Geophysical Engineering*. 8, 342-345.

Nama Pardaz Rayaneh. Available online: (2017) URL www.nprco.com

Nguyen, V-N., Yariyan, P., Amiri, M., Dang Tran, A., Pham, T.D., Do, MP., Thi Ngo, P.T., Nhu, V-H., Quoc Long, N., & Tien Bui, D. (2020). A New Modeling Approach for Spatial Prediction of Flash Flood with Biogeography Optimized CHAID Tree Ensemble and Remote Sensing Data. *Remote Sensing*. 12,1373.

Niedzielski, T., Witek, M., & Spallek, W. (2016). Observing river stages using unmanned aerial vehicles. *Hydrology and Earth System Sciences*. 20, 3193-3205.

Perks, M.T., Russell, A.J., & Large, A.R. (2016). Advances in flash flood monitoring using unmanned aerial vehicles (UAVs). *Hydrology and Earth System Sciences*. 20, 4005-4015.

Popescu, D., Ichim, L., & Stoican, F. (2017). Unmanned aerial vehicle systems for remote estimation of flooded areas based on complex image processing. *Sensors.* 17, 446.

Rahman, M.M., & Ali, M.M. (2016). Flood Inundation Mapping of Floodplain of the Jamuna River using HEC-RAS and HEC-GeoRAS. *Presidency*. 3, 24-32.

Ridolfi, E., Rianna, M., Trani, G., Alfonso, L., Di Baldassarre, G., Napolitano, F., & Russo, F. (2016). A new methodology to define homogeneous regions through an entropy-based clustering method. *Advances in water resources.* 96, 237-250.

Rong, Y., Zhang, T., Zheng, Y., Hu, C., Peng, L., & Feng, P. (2019). Three-dimensional urban flood inundation simulation based on digital aerial photogrammetry. *Journal of Hydrology*, 124308.

Salimi, ET., Nohegar, A., Malekian, A., Hoseini, M., & Holisaz, A. (2017). Estimating time of concentration in large watersheds. *Paddy and water environment*. 15, 123-132.

Salimi Kouchi, H., Sahebi, M.R., Abkar, AA, & Valadan Zoej, M.J. (2013). Fractional vegetation cover estimation in urban environments. *ISPRS-International Archives of the Photogrammetry, Remote Sensing and Spatial Information Sciences*. 3, 357-360.

Schumann, G.J. P., Muhlhausen, J., & Andreadis, K.M. (2019). Rapid mapping of small-scale river-floodplain environments using UAV SfM supports classical theory. *Remote Sensing*. 11, 982.

Şerban, G., Rus, I., Vele, D., Breţcan, P., Alexe, M., & Petrea, D. (2016). Flood-prone area delimitation using UAV technology, in the areas hard-to-reach for classic aircrafts: case study in the north-east of Apuseni Mountains, Transylvania. *Natural Hazards*. 82, 1817-1832.

Sensefly Company. Available online : (2020) URL https://www.sensefly.com/

Sivapalan, M., Takeuchi, K., Franks, S.W., Gupta, V.K., Karambiri, H., Lakshmi, V., & Oki, T. (2003). IAHS Decade on Predictions in Ungauged Basins (PUB), 2003–2012: Shaping an exciting future for the hydrological sciences. *Hydrological sciences journal*. 48, 857-880.

Sumalan, A. L., Popescu, D., & Ichim, L. (2017). Flooded and vegetation areas detection from UAV images using multiple descriptors. *21st International Conference on System Theory, Control and Computing (ICSTCC)*. 447-452.

Tauro, F., Porfiri, M., & Grimaldi, S. (2014). Orienting the camera and firing lasers to enhance large scale particle image velocimetry for streamflow monitoring. *Water Resources Research*. 50, 7470-7483.

The university of texas at Austin (Civil, Architectural and Environmental Engineering). Available online: (1997). URL http://www.ce.utexas.edu/prof/maidment/gishydro/ferdi/research/agree/agree.html

Tokarczyk, P., Leitão, J.P., Rieckermann, J., & Blumensaat, F. (2015). High-quality observation of surface imperviousness for urban runoff modelling using UAV imagery. *Hydrology and Earth System Sciences*. 19, 4215-4228.

Watanabe, Y., & Kawahara, Y. (2016). UAV photogrammetry for monitoring changes in river topography and vegetation. *Procedia Engineering*. 154, 317-325.

Weng, Q. (2012). Remote sensing of impervious surfaces in the urban areas: Requirements, methods and trends. *Remote sensing of Environment*. 117, 34-49.

Yalcin, E. (2018). Generating of high-resolution digital surface models for urban flood modeling using UAV imagery. *WIT Transactions on Ecology and the Environment*. 215, 357-366.

Yahya, BM., Devi, N.M., & Umrikar, B. (2010). Flood hazard mapping by integrated GIS-SCS model. *International Journal of Geomatics and Geosciences*. 1, 489.

Zazo, S., Molina, J.L., & Rodríguez-Gonzálvez, P. (2015). Analysis of flood modeling through innovative geomatic methods. *Journal of Hydrology*. 524, 522-537.

Zeleňáková, M., Fijko, R., Labant, S., Weiss, E., Markovič, G., & Weiss, R. (2019). Flood risk modelling of the Slatvinec stream in Kružlov village, Slovakia. *Journal of cleaner production*. 212, 109-118.